

Weak lensing, dark matter and dark energy

Dragan Huterer

Received: date / Accepted: date

Abstract Weak gravitational lensing is rapidly becoming one of the principal probes of dark matter and dark energy in the universe. In this brief review we outline how weak lensing helps determine the structure of dark matter halos, measure the expansion rate of the universe, and distinguish between modified gravity and dark energy explanations for the acceleration of the universe. We also discuss requirements on the control of systematic errors so that the systematics do not appreciably degrade the power of weak lensing as a cosmological probe.

Keywords Cosmology · Weak Gravitational Lensing · Dark Matter · Dark Energy

1 Introduction

Within the past decade, weak gravitational lensing — slight distortions of galaxy images due to the bending of the light from distant galaxies by the intervening large-scale structure — has become one of the principal probes of cosmology. The weak lensing regime corresponds to the intervening surface density of matter being much smaller than some critical value. While weak lensing around individual massive halos was measured in the 1990s [1, 2], weak lensing by large-scale structure was eagerly expected, its signal predicted by theorists around the same time [3, 4, 5, 6, 7, 8, 9]. In this latter regime, the observed galaxies are slightly distorted (roughly at the 1% level) and one needs a large sample of foreground galaxies in order to separate the lensing effect from the noise represented by random orientations of galaxies. A watershed moment came in the year 2000 when four research groups nearly simultaneously announced the first detection of weak lensing by large-scale structure [10, 11, 12, 13]. Since that time, weak lensing has grown into an increasingly accurate and powerful probe of dark matter and dark energy.

Dragan Huterer
Physics Department
University of Michigan
450 Church St.
Ann Arbor, MI 48109
E-mail: huterer@umich.com

The principal power of weak lensing comes from the fact that it responds only to dark matter, and not to visible (or, more generally, baryonic) matter like most other probes of the large-scale structure. Therefore, modeling of the visible-to-dark matter bias, a thorny and complicated subject, is altogether avoided when using weak lensing. Simulations of dark matter clustering are becoming increasingly accurate, and in principle there is no reason why simulation-based predictions cannot reach the accuracy required to model the weak lensing signal so that modeling errors do not appreciably contribute to the total error budget. Because of our ability to model its signal accurately, weak lensing has great intrinsic power to probe dark matter and dark energy in the universe.

The other principal reason why weak lensing is powerful comes from the nature of its observable quantity. Galaxy shear is measured relatively straightforwardly, and comes from millions of galaxies typically observed in current surveys. While *individual* galaxy shear measurements do not provide cosmological information, correlation of galaxy shear across the sky does, especially if redshift information of galaxies is utilized to obtain 3-dimensional “tomography”. In fact, shear-shear correlations can be used to obtain stringent constraints on cosmological parameters *and* use information from the survey to control the systematic errors at the same time.

In this article, we briefly review the physics of how weak lensing probes dark matter and dark energy. Our emphasis is on the latter, as dark energy has emerged as the principal mystery of physics and cosmology (for a review of dark energy, see [14]). The discovery of dark energy and observations of weak lensing are both about a decade old, and there have been numerous investigations in recent years as to how best to use weak lensing to probe dark energy. This is a condensed review of the subject; for a more extensive treatment of weak lensing, we recommend excellent reviews by Mellier [15], Bartelmann and Schneider [16], Refregier [17], Munshi et al. [18], and Hoekstra and Jain [19].

2 Weak lensing basics

2.1 Theoretical foundations

In Newtonian Gauge the perturbed Friedmann-Robertson-Walker metric reads

$$ds^2 = -(1 + 2\Psi) dt^2 + a^2(t) (1 - 2\Phi) \left[d\chi^2 + r^2(d\theta^2 + \sin^2 \theta d\phi^2) \right] \quad (1)$$

where χ is the radial coordinate, θ and ϕ are angular coordinates, a is the scale factor, and we have set $c = 1$. Here $r(\chi)$ is the comoving distance; in the special case of a flat universe, $r(\chi) = \chi$. Finally Φ and Ψ are the gravitational potentials, and $\Phi \simeq \Psi$ in General Relativity and in the absence of anisotropic stresses.

Gravitational lensing produces distortions of images of background galaxies. These distortions can be described as mapping between the source plane (S) and the image plane (I) [20]

$$\delta x_i^S = A_{ij} \delta x_j^I, \quad (2)$$

where $\delta \mathbf{x}$ are the displacement vectors in the two planes and A is the distortion matrix

$$A = \begin{pmatrix} 1 - \kappa - \gamma_1 & -\gamma_2 \\ -\gamma_2 & 1 - \kappa + \gamma_1 \end{pmatrix}. \quad (3)$$

The deformation is described by the convergence κ and complex shear $\gamma = \gamma_1 + i\gamma_2$. We are interested in the weak lensing limit, where $|\kappa|, |\gamma| \ll 1$. The convergence in any particular direction on the sky $\hat{\mathbf{n}}$ is given by the integral along the line-of-sight

$$\kappa(\hat{\mathbf{n}}, \chi) = \int_0^\chi W(\chi') \delta(\chi') d\chi', \quad (4)$$

where δ is the relative perturbation in matter density and

$$W(\chi) = \frac{3}{2} \Omega_M H_0^2 g(\chi) (1+z) \quad (5)$$

is a weight function, Ω_M is the matter energy density relative to critical, H_0 is the Hubble constant, and z is the redshift. Furthermore

$$g(\chi) = r(\chi) \int_\chi^\infty d\chi' n(\chi') \frac{r(\chi' - \chi)}{r(\chi')} \rightarrow \frac{r(\chi)r(\chi_s - \chi)}{r(\chi_s)}, \quad (6)$$

where $n(\chi)$ is the radial distribution of source galaxies (normalized so that $\int d\chi n(\chi) = 1$) and the equality that follows the arrow holds only if all sources are at a single redshift z_s . The distribution of source galaxies often follows a bell-shaped curve whose peak redshift depends on the depth of the survey.

The quantity that is most easily determined from observations is shear, which is directly related to the ellipticity of the observed galaxy (in the weak lensing limit, shear is approximately equal to the average ellipticity). Shear is given by

$$\gamma \equiv \gamma_1 + i\gamma_2 = \frac{1}{2} (\psi_{,11} - \psi_{,22}) + i\psi_{,12} \quad (7)$$

where ψ is the projected Newtonian potential, $\psi_{,ij} = -(1/2) \int g(\chi) (\Psi_{,ij} + \Phi_{,ij}) d\chi$, and commas denote derivatives with respect to directions perpendicular to the line of sight. Unfortunately, this quantity is not easily related to the distribution of matter in the universe and the cosmological parameters. Convergence, on the other hand, is given by

$$\kappa = \frac{1}{2} (\psi_{,11} + \psi_{,22}) \quad (8)$$

which can be directly related to the distribution of matter (see Eq. (4)), and is convenient for comparison with theory. However, it is very difficult to measure the convergence itself, as convergence depends on the magnification of galaxies which would need to be measured.

Measurements of ellipticities of distant galaxies can be used to reconstruct the ‘‘reduced shear’’ $\gamma/(1 - \kappa)$, which is approximately equal to shear γ in the weak lensing limit (for the potential deleterious effects of assuming this approximation when estimating cosmological parameters, see [21]). Measurements of shear are complicated by atmospheric effects such as blurring by the atmosphere, the fact that shapes of galaxies are irregular and not perfectly elliptical, shearing due to the instrument, etc. Correction of these effects and minimization of the underlying biases are very important. Recently, impressive attempts to find agreement between different shear estimators have been made in the weak lensing community with the Shear TEsting Programme (STEP [22, 23]).

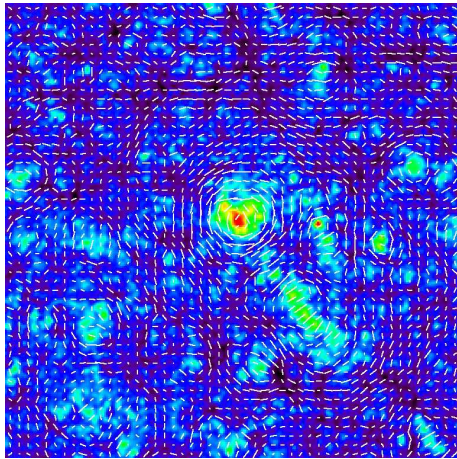


Fig. 1 Cosmic shear field (white ticks) superimposed on the projected mass distribution from a cosmological N-body simulation: overdense regions are bright, underdense regions are dark. Note how the shear field is correlated with the foreground mass distribution. Figure courtesy of T. Hamana.

2.2 Shear/convergence power spectrum and tomography

While individual galaxy shear (or convergence) cannot be predicted theoretically, statistical *correlations* of galaxy shears can. Transforming the convergence into multipole space

$$\kappa_{\ell m} = \int d\hat{\mathbf{n}} \kappa(\hat{\mathbf{n}}, \chi) Y_{\ell m}^*, \quad (9)$$

and assuming statistical isotropy, the power spectrum of convergence P_{ℓ}^{κ} is then defined as the harmonic transform of the two-point correlation function of the convergence

$$\langle \kappa_{\ell m} \kappa_{\ell' m'} \rangle = \delta_{\ell_1 \ell_2} \delta_{m_1 m_2} P^{\kappa}(\ell). \quad (10)$$

The convergence power spectrum is identical to the shear power spectrum in the limit of weak distortions; $P^{\gamma}(\ell) \simeq P^{\kappa}(\ell)$. Either quantity is the observable quantity that contains a lot of information about the weak lensing field. In the limit of a Gaussian field, the two point function would contain all information; however, since the weak lensing field is nongaussian on small scales, higher-order correlations are important; see the next subsection.

Weak lensing tomography — slicing of the shear signal in redshift bins — enables extraction of additional information from the weak lensing shear, as it makes use of the radial information [24]. Consider correlating shears in some redshift bin i to those in the redshift bin j . The tomographic cross-power spectrum for these two redshift bins, at a given multipole ℓ , is defined by

$$\langle \kappa_{\ell m, i} \kappa_{\ell' m', j} \rangle = \delta_{\ell_1 \ell_2} \delta_{m_1 m_2} P_{ij}^{\kappa}(\ell). \quad (11)$$

and can be related to theory via [4, 7, 24]

$$P_{ij}^{\kappa}(\ell) = \int_0^{\infty} dz \frac{W_i(z) W_j(z)}{r(z)^2 H(z)} P\left(\frac{\ell}{r(z)}, z\right), \quad (12)$$

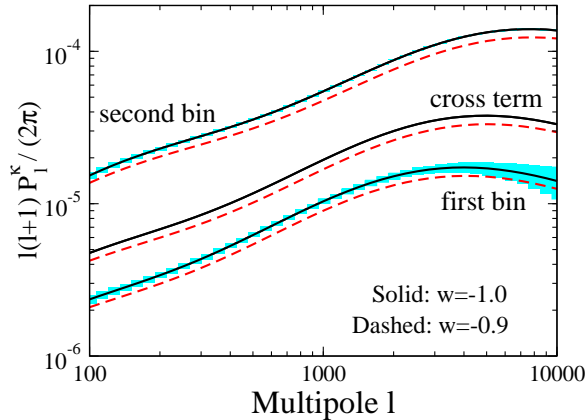


Fig. 2 Cosmic shear angular power spectrum and statistical errors expected for LSST for $w = -1$ and -0.9 . For illustration, results are shown for source galaxies in two broad redshift bins, $z_s = 0-1$ (first bin) and $z_s = 1-3$ (second bin); the cross-power spectrum between the two bins (cross term) is shown without the statistical errors. We employ the redshift distribution of galaxies of the form $n(z) \propto z^2 \exp(-z/z_0)$ that peaks at $2z_0 = 1.0$. Adopted from Ref. [14].

where $r(z)$ is the comoving angular diameter distance and $H(z)$ is the Hubble parameter. The weights W_i are given by $W_i(\chi) = \frac{3}{2} \Omega_M H_0^2 g_i(\chi) (1+z)$ where $g_i(\chi) = r(\chi) \int_{\chi}^{\infty} d\chi_s n_i(\chi_s) r(\chi_s - \chi) / r(\chi_s)$, and n_i is the comoving density of galaxies if χ_s falls in the distance range bounded by the i th redshift bin and zero otherwise. The observed convergence auto-correlation power spectrum has additional contribution from the shot noise given by random galaxy shapes

$$C_{ij}^{\kappa}(\ell) = P_{ij}^{\kappa}(\ell) + \delta_{ij} \frac{\langle \gamma_{\text{int}}^2 \rangle}{\bar{n}_i}, \quad (13)$$

where $\langle \gamma_{\text{int}}^2 \rangle^{1/2}$ is the rms intrinsic shear in each component (which is typically around 0.2), and \bar{n}_i is the average number of galaxies with well-measured shapes in the i th redshift bin per steradian. Clearly, the more galaxies there are and the fewer their intrinsic ellipticities are, the smaller the shot noise will be.

The statistical uncertainty in measuring the shear power spectrum is [4, 7]

$$\Delta P_{ij}^{\kappa}(\ell) = \sqrt{\frac{2}{(2\ell+1)f_{\text{sky}}}} \left[P_{ij}^{\kappa}(\ell) + \frac{\langle \gamma_{\text{int}}^2 \rangle}{\bar{n}_i} \right], \quad (14)$$

where f_{sky} is the fraction of sky area covered by the survey. The first term in brackets, which dominates on large scales, comes from cosmic variance of the mass distribution, and the second, shot-noise term results from both the variance in galaxy ellipticities (“shape noise”) and from shape-measurement errors due to noise in the images. Fig. 2 shows the dependence on the dark energy of the shear power spectrum and an indication of the statistical errors expected for a survey such as Large Synoptic Survey Telescope (LSST [25]), assuming a survey area of 15,000 sq. deg.

2.3 Three-point correlation function of shear/convergence

The two-point correlation function has been by far the most analyzed, and so far best measured, weak lensing statistic. However, higher-order correlation functions also contain significant cosmological information; chief among these is the three-point correlation function. With purely Gaussian shear or convergence field, the three-point function is of course zero (within measurement and cosmic-variance errors). While primordial nongaussianity can produce a nonzero three-point function, nonlinear clustering of structure presents the most widely anticipated — and in fact guaranteed — signal in the three-point function [6, 26, 27, 28, 29, 30].

The three-point correlation function of the convergence in multipole space can be related to the bispectrum of the convergence $B_{\ell_1 \ell_2 \ell_3}^\kappa$ via

$$\langle \kappa_{\ell_1 m_1} \kappa_{\ell_2 m_2} \kappa_{\ell_3 m_3} \rangle = \begin{pmatrix} \ell_1 & \ell_2 & \ell_3 \\ m_1 & m_2 & m_3 \end{pmatrix} B_{\ell_1 \ell_2 \ell_3}^\kappa \quad (15)$$

where the term in parentheses is the Wigner 3j symbol. The convergence bispectrum is essentially a projection along the line of sight of the matter overdensity bispectrum

$$B_{\ell_1 \ell_2 \ell_3}^\kappa = \sqrt{\frac{(2\ell_1 + 1)(2\ell_2 + 1)(2\ell_3 + 1)}{4\pi}} \begin{pmatrix} \ell_1 & \ell_2 & \ell_3 \\ 0 & 0 & 0 \end{pmatrix} \times \left[\int dz \frac{[W(z)]^3}{r(z)^4 H(z)} B \left(\frac{\ell_1}{r(z)}, \frac{\ell_2}{r(z)}, \frac{\ell_3}{r(z)}, z \right) \right] \quad (16)$$

where $W(z)$ is the same weight function as in Eq. (12). The (convergence) bispectrum is defined only if the following relations are satisfied: $|\ell_j - \ell_k| \leq \ell_i \leq |\ell_j + \ell_k|$ for $\{i, j, k\} \in \{1, 2, 3\}$ and $\ell_1 + \ell_2 + \ell_3$ is even. To compute the bispectrum of the convergence, therefore, we need to supply the matter bispectrum $B(k_1, k_2, k_3, z)$ which, on mildly nonlinear scales of interest, can be evaluated using the halo model or perturbation theory techniques, or else calibrated directly from cosmological N-body simulations.

Measurements (and detections) of the three-point function have been first made in the VIRMOS-DESCART survey [31, 32], and, more recently, in the COSMOS survey [33]. Much better constraints are anticipated from future wide-field surveys [34]. However, including the covariance between the power spectrum and the bispectrum — a difficult quantity to estimate in its own right — may degrade the combined constraints relative to a naive (i.e. uncorrelated) combination of their constraints [35].

3 Galaxy-galaxy lensing and galaxy cluster counts

One effective application of weak lensing is to measure the correlation of shear of the background galaxies with mass of the foreground galaxies. This method goes under the name of “galaxy-galaxy lensing” [2, 36, 37, 38, 39], and essentially measures the galaxy-shear correlation function across the sky. Galaxy-galaxy lensing measures the surface mass density contrast $\Delta\Sigma(R)$

$$\Delta\Sigma(R) \equiv \overline{\Sigma}(< R) - \overline{\Sigma}(R) = \Sigma_{\text{crit}} \times \gamma_t(R). \quad (17)$$

$\overline{\Sigma}(< R)$ is the mean surface density within proper radius R , $\overline{\Sigma}(R)$ is the azimuthally averaged surface density at radius R (e.g. [3, 40]), γ_t is the tangentially projected shear,

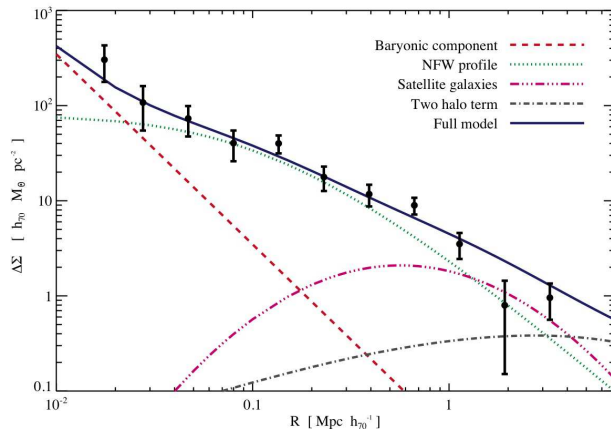


Fig. 3 Surface density profile measurements obtained from galaxy groups in the COSMOS survey [44, 45]. The legend shows various components of the halo model fit to the profile. Figure kindly provided by Alexie Leauthaud.

and the critical surface density Σ_{crit} is a known function of the distances to the source and the lens. The surface density can be further inverted to obtain radial density profiles of dark matter halos [41, 42]. More accurate modeling of the galaxy-galaxy lensing signal, that takes into account clustering with other halos and the baryonic content of each halo, can be done using the halo model of large scale structure [43]. Figure 3 shows the surface density profile of a sample of ~ 600 galaxies in the COSMOS survey with stellar masses of order $\sim 10^{11} M_{\odot}$ and at $z \sim 0.5$, together with halo model fits [44, 45]. Current measurements constrain the density profiles and bias of dark matter halos [41, 46, 47, 48], and the relation between their masses and luminosities [49, 50]. In the future, galaxy-shear correlations have potential to constrain dark energy models [51] and modified gravity models for the accelerating universe [52].

Weak lensing signal can also be used to *detect* and count massive halos — particularly galaxy clusters. This method, pioneered recently [53, 54], can be used to obtain cluster samples whose masses are reliably determined, avoiding the arguably more difficult signal-to-mass conversions required with the X-ray or optical observations [55, 56, 57, 58]. Much important information about the dark matter and gas content of galaxy clusters can be inferred with the combined lensing, X-ray and optical observations. This has recently been demonstrated with observations of the “Bullet” cluster [59], where the dark matter distribution inferred from weak lensing is clearly offset from the hot gas inferred from the X-ray observations (see Fig. 4), indicating the presence and distinctive fingerprints of dark matter.

Finally, one can use the abundance clusters detected through weak lensing to constrain cosmological parameters (e.g. [60, 61]). The number of halos of in the mass range $[M, M + dM]$ in a patch of the sky with solid angle $d\Omega$ and in a redshift interval $[z, z + dz]$ is given by

$$\frac{d^2 N}{d\Omega dz} = \frac{r^2(z)}{H(z)} \frac{dn(M, z)}{dM} dM \quad (18)$$

where $r(z)$ and $H(z)$ are the comoving distance and the expansion rate respectively, and $n(M, z)$ is the number density (the “mass function”) that can be calibrated from

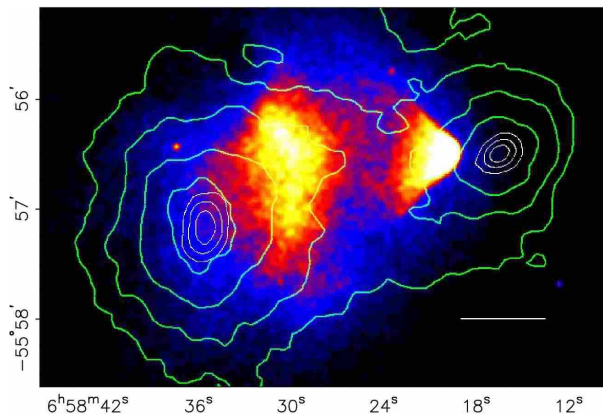


Fig. 4 X-ray emission from the “Bullet” cluster of galaxies observed by ground and space telescopes. Colored features correspond to X-ray emission observed by Chandra space telescope, while the green contours correspond to mass reconstruction from weak lensing observations. The “bullet” is a smaller subcluster which has passed through the larger cluster and whose hot gas is seen in X-rays, being clearly distinct from the total mass of the system. Adopted from Ref. [59].

numerical simulations. Because weak lensing signal is directly sensitive to the cluster mass, the usual uncertainty in mapping from the observable signal (X-ray, or optical light, etc) and mass is largely avoided. However, contamination of the cluster shear by the projected mass (i.e. large-scale structures between us and the cluster) can seriously degrade the effectiveness of lensing-detected cluster counts (e.g. [62]). It is therefore necessary to use N-body simulations to calibrate purity (contribution of false detections) and completeness (fraction of detections relative to the truth) of the shear peaks [63, 64, 65, 66, 67, 68, 69], and the jury is still out as to whether the projection systematics can be controlled to sufficient accuracy. An alternative to using the weak-lensing-detected clusters is to apply weak lensing mass measurements to clusters detected via X-ray [70] or optical [71] observations.

4 Cosmological constraints

First detections of weak lensing by large-scale structure have been announced nearly a decade ago [10, 11, 12, 13]. Their results were in mutual agreement and consistent with theoretical expectations, which is remarkable given that they were obtained independently. Meanwhile, additional measurements have been collected using ground-based [72, 73, 74, 75, 76, 77, 78] and space-based [79, 80, 44, 81] observations, leading to increasingly better understanding of systematic errors.

4.1 Current constraints

Current ground-based weak lensing surveys cover of order ~ 100 square degrees. Space-based surveys currently cover only a few square degrees, but utilize significantly more distant galaxies whose lensing signal is more pronounced.

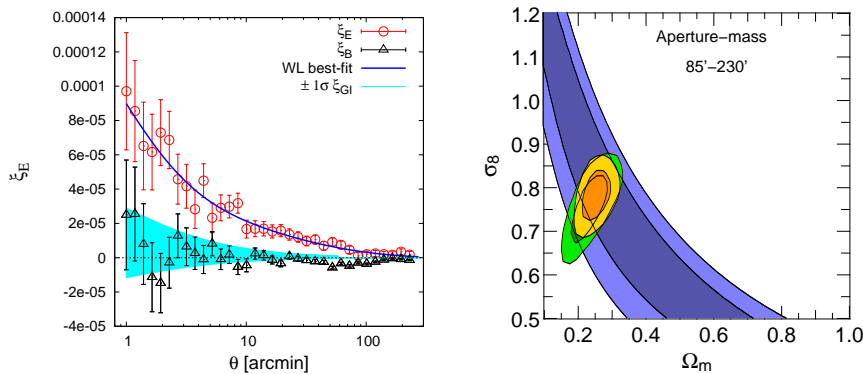


Fig. 5 Example of cosmological constraints from weak lensing data, adopted from Canada-France-Hawaii Telescope Legacy Survey (CFHTLS; [84]). *Left panel:* E and B mode measurements; note that B modes are consistent with zero, and their scatter is consistent with expectations from the alignment between intrinsic shapes of galaxies. *Right panel:* Constraints (68% and 95% confidence) in the Ω_M - σ_8 plane. Blue contours are from weak lensing, green contours are from the CMB (WMAP 3-year; [85]), and the orange contours are the two combined. Adopted from Ref. [84].

Modest sky coverage of current surveys, combined with evolving understanding of the systematic errors, means that only a few parameter combinations can be measured to an interesting accuracy as of this writing. In particular, the combination $\sigma_8 \Omega_M^{0.6}$, where σ_8 is the amplitude of mass fluctuations, is measured to about 5-10% from the ground [82,78] and $\sim 15\%$ from space [83], and is in concordance with values of $\Omega_M \simeq 0.25$ and $\sigma_8 \simeq 0.8$. An example adopted from Ref. [84] is shown in Fig. 5, with measurements of E and B mode correlation functions of shear in real space (left panel), and the resulting constraints on σ_8 and Ω_M (right panel). Such constraints are impressive given that first detections of weak lensing by large-scale structure have been made less than a decade ago.

Weak lensing also probes dark energy, though at the present time it needs to be combined with other cosmological probes in order to produce interesting constraints on the equation of state w . Recent work illustrates how weak lensing helps tighten the constraints from SNe Ia and CMB [86] mostly due to its sensitivity to growth of density perturbations. It is also possible to place constraints on specific dark energy model from current weak lensing data [87]. Upcoming weak lensing surveys from the ground and space hold promise to measure dark energy significantly better, as we now discuss.

4.2 Future constraints

The errors in the cosmological constraints can then be easily and straightforwardly forecasted using the Fisher matrix formalism. Consider a set of cosmological parameters p_i ($i = 1, \dots, N_{\text{par}}$) and weak lensing observations that result in measurements of the shear power spectrum $C_{jk}^{\kappa}(\ell)$, defined in Eq. (13) and where j and k run over the

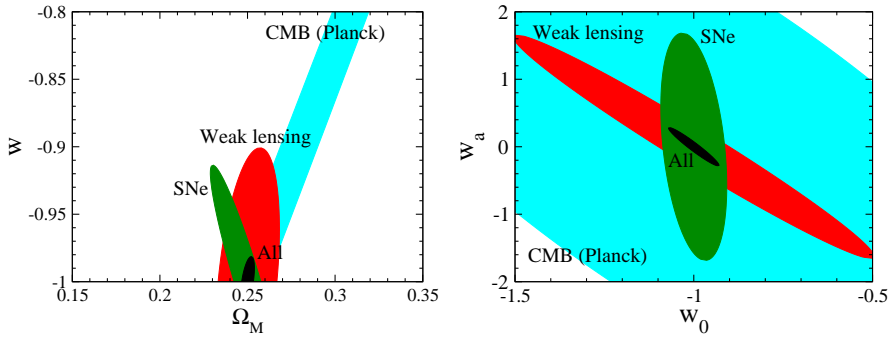


Fig. 6 Illustration of forecast constraints on dark energy parameters, adopted from Ref. [14]. Shown are 68% C.L. uncertainties for one version of the proposed SNAP experiment, which combines a narrow-area survey of 2000 SNe to $z = 1.7$ and a weak lensing survey of 1000 sq. deg. *Left panel:* Constraints in the Ω_M - w plane, assuming constant w ; the vertical axis can also be interpreted as the pivot value w_p for a time-varying equation of state. *Right panel:* Constraints in the w_0 - w_a plane for time-varying dark energy equation of state, marginalized over Ω_M for a flat Universe.

tomographic redshift bins. Then the Fisher matrix is defined as

$$F_{ij} = \sum_{\ell} \frac{\partial \mathbf{C}}{\partial p_i} \mathbf{Cov}^{-1} \frac{\partial \mathbf{C}}{\partial p_j}, \quad (19)$$

where \mathbf{C} is the column matrix of the observed power spectra and \mathbf{Cov}^{-1} is the inverse of the covariance matrix between the observed power spectra whose elements are given by

$$\text{Cov} [C_{ij}^{\kappa}(\ell), C_{kl}^{\kappa}(\ell')] = \frac{\delta_{\ell\ell'}}{(2\ell+1)f_{\text{sky}}} [C_{ik}^{\kappa}(\ell)C_{jl}^{\kappa}(\ell) + C_{ii}^{\kappa}(\ell)C_{jk}^{\kappa}(\ell)]. \quad (20)$$

assuming that the convergence field is Gaussian, which is a good approximation at $\ell \lesssim 3000$. By the Kramer-Rao inequality, cosmological parameters can typically be measured to no better than $\sigma(p_i) = 1/\sqrt{F_{ii}}$ (unmarginalized error), or $\sigma(p_i) = \sqrt{(F^{-1})_{ii}}$ (marginalized over all other parameters). In practice, these idealistic error bars are usually a good approximation to the truth if the parameters are sufficiently well measured so that their covariances are ellipsoid-shaped and not “banana-shaped” regions.

Weak lensing measurements can determine cosmological parameters to an excellent accuracy due to the fact that modeling the weak lensing signal only requires modeling of dark matter, though baryonic collapse at centers of dark matter halos and galaxy alignments complicate the picture somewhat and contribute to systematic errors discussed below.

First cosmological parameter accuracy projections from weak lensing have been made in [88] while increasingly more sophisticated estimates [89,90,34,91,92,93,94,95,96] indicate prospects for determining the parameter σ_8 to much better than 1% and the equation of state of dark energy to a few percent accuracy in the future. An example of such projections is shown in Fig. 6, where we show constraints on Ω_M and constant w (left panel) and w_0 and w_a (right panel) from SuperNova/Acceleration probe (SNAP [97]), a proposed space-based experiment to probe dark energy. These constraints marginalize over ~ 5 other cosmological parameters, and allow for the presence of systematic as well as statistical errors.

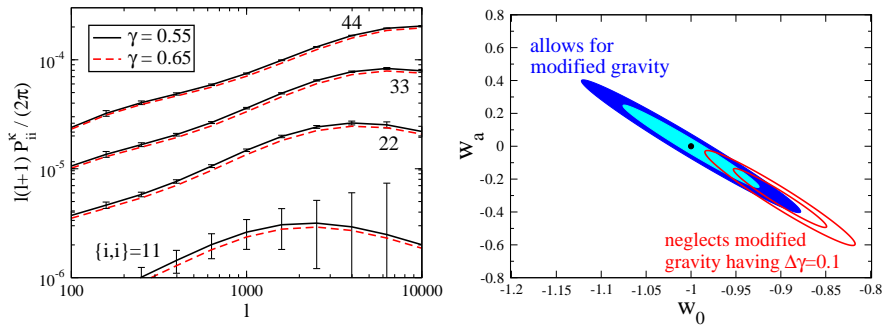


Fig. 7 Example of how weak lensing can constrain modifications of gravity parametrized by the growth index γ , adopted from Ref. [103]. *Left panel:* Auto-correlation power spectra of 4-bin weak lensing tomography for the two values of the growth index, with statistical errors shown for the $\gamma = 0.55$ model. This shows that a relatively small signal due to modified gravity can be detected using future weak lensing observations. *Right panel:* Bias in constraints in cosmological parameters w_0 and w_a if changes in modified gravity were ignored, for the $\Delta\gamma = 0.1$ modification relative to the fiducial model. Recall, the growth index in DGP braneworld gravity differs from the General Relativity value by $\Delta\gamma \approx 0.67 - 0.55 = 0.12$.

Finally, we mention the proposed technique to correlate the mass of foreground galaxies with the shear of the background galaxy population, and thus isolate geometric distance factors in photometric redshift bins. This approach sometimes goes under the name of “cross-correlation cosmography” [98], and is very closely related to galaxy-galaxy lensing. Cross-correlation cosmography is potentially less sensitive to systematic errors as well as assumptions about the nonlinear clustering of dark matter than the shear-shear correlation measurements, and can significantly complement cosmological constraints obtained from the latter. [98, 99, 100, 101, 102, 51]

5 Weak Lensing and Modified Gravity

Weak lensing is a particularly effective discriminator of modified gravity explanations for the accelerating universe. Modified gravity stipulates that the reason for the apparent acceleration are modifications to General Relativity on large scales (e.g. in the infrared). General Relativity has to be preserved on the solar-system and galactic scales in order to satisfy stringent observational constraints, but modifications on large scales could masquerade as an *apparent* acceleration when the equations of standard Einstein’s gravity are used to interpret the observations.

Gravitational lensing is particularly useful probe of modified gravity because it probes the sum of the two gravitational potentials $\Phi + \Psi$ (see Eq. (1)), while particle dynamics probes Ψ alone (e.g. [104, 105]). Since modifications to gravity typically affect the potentials differently, combination of weak lensing with other cosmological probes can in principle be used to differentiate modified gravity from dark energy. For a detailed review of how weak lensing can be used to test gravity, see the review [106] in this Special Issue.

The simplest approach to distinguish between modified gravity and honest-to-god dark energy is to parametrize anomalous growth of density perturbations; the most

popular approach is via the “growth index” parameter [107]. The linear growth factor $g(a) \equiv \delta(a)/a$ (scaling out the matter dominated universe behavior $\delta \propto a$), where a is the scale factor, is approximated by

$$g(a) = e^{\int_0^a d \ln a [\Omega_M(a)^\gamma - 1]}, \quad (21)$$

where γ is a new parameter called the growth index (not to be confused with shear!). This fitting function is accurate to 0.3% compared to the exact solution within general relativity for a wide variety of physical dark energy equation of state ratios including equations of state $w(a) = w_0 + w_a(1 - a)$, provided that the function takes the value $\gamma = 0.55 + 0.05(1 + w(z = 1))$ [107]. The fitting formula also fits [108] the linear growth in the popular “braneworld gravity” model of Dvali, Gabadadze and Porrati (DGP [109]), but with a different value of the growth index, $\gamma \simeq 0.67$. More generally, measuring γ can distinguish between modified gravity and dark energy even if the two predict identical expansion history (e.g. distances in the universe; for a similar approach not using the growth index, see [110, 111]). Future expectations are for γ to be measured to accuracy of about 0.02-0.03 from weak lensing data combined with other cosmological probes that measure the distance scale (SNe Ia, CMB) or growth (cluster abundance) [103, 112]; see Fig. 7 for an example.

Weak lensing can also probe specific models where dark matter or dark energy interactions are modified. For example, models of massive gravity, where the Poisson equation is phenomenologically modified with the Yukawa term, have been constrained with weak lensing observations [113, 114]; preliminary constraints have been imposed on some other models as well [115]. In the future, weak lensing data will enable a much more ambitious battery of tests of modified gravity, essentially enabling comparison of distance and growth functions at multiple redshifts and on multiple angular scales [116, 117, 118, 119].

6 Second-order effects as a signal for cosmology

So far we have discussed weak lensing of galaxies by the large-scale structure, a principal signature of weak lensing used in cosmology. However, objects other than galaxies are also weakly lensed, and their properties can sometimes be used to our advantage.

In particular, high- z type Ia supernovae (SN Ia) will be gravitationally lensed by the foreground large-scale structure. The useful property of SN Ia is that they have nearly uniform intrinsic luminosities. Weak lensing will magnify SN Ia and perturb these luminosities, and the resulting magnifications will be correlated and may be measurable with future surveys. The resulting magnification of supernova luminosity distance is

$$\mu = [(1 - \kappa)^2 - |\gamma|^2]^{-1} \approx 1 + 2\kappa + 3\kappa^2 + |\gamma|^2 + \dots, \quad (22)$$

where κ is the lensing convergence and $|\gamma| = \sqrt{\gamma_1^2 + \gamma_2^2}$ is the total shear at the angular location of the SN. Each supernova’s luminosity L and distance d_L will be perturbed as $\delta L/L = 2|\delta d_L/d_L| = \mu - 1$, where μ is magnification at that location and out to redshift of the SN. The magnification of SN — really, the correlated pattern of the departures of their observed distances from the true values — comes for free with standard measurements of SN distances to measure the expansion history of the universe.

Measurements of cosmic magnification of supernovae therefore complement galaxy shear measurements in providing a direct measure of clustering of the dark matter [120]. As the number of supernovae is typically much smaller than the number of galaxies, the two-point correlation function of lensed SN Ia is more noisy than, and not as effective as, the galaxy shear. However, weak lensing of SN Ia probes magnification directly, and can be used to measure the second-order corrections in Eq. (22) between magnification and convergence (or equivalently, shear and convergence) [120]. Additionally, the power spectrum of magnification can be used to measure the cosmological parameters such as σ_8 [121]. While this application of weak lensing is rather challenging and requires a large number of SN Ia to be effective, we emphasize that it comes for free in wide-field surveys that measure galaxy shear as well as SN Ia, and combines weak lensing shear and magnification information in the same field, providing a number of cross checks on the systematics.

7 Systematic errors and their calibration requirements

Because weak lensing has so much statistical power, it is imperative to control the systematic errors so that they do not appreciably degrade the statistical errors on the weak lensing power spectrum (see e.g. the small error bars in Fig. 2), and the similarly small errors on the cosmological parameters (see Fig. 6).

7.1 Observational errors

One of the most important systematic effects on weak lensing are the photometric redshift errors — uncertainties in measuring redshifts of sheared galaxies. For weak lensing measurements that simply integrate signal along the line of sight, redshift errors are clearly not critically important, as only the overall radial distribution of galaxies, $n(z)$, needs to be known (see Eq. 6). However, for tomographic measurements, the photometric redshift errors lead to leakage of galaxies from their original redshift bin and contamination of signal in the bin where they are misplaced.

The required accuracy of photometric redshift bins has been studied in detail [122]; and it was found that the mean and spread of the relation between photometric and (true) spectroscopic redshift, *averaged* over bins of $\Delta z = 0.1$, both need to be *known* to better than about 0.003 [122]; see the right panel of Fig. 8. While errors in individual galaxy redshift are greater than this by about an order of magnitude, it is reasonable to expect that modern photometric redshift techniques (e.g. [123]) can achieve this required accuracy in each redshift bin. Moreover, a possibility of *catastrophic* redshift errors — cases where the true redshift is misestimated by a significant amount — is equally troubling, and requires knowledge of outlier “islands” in the $z_{\text{spec}}-z_{\text{phot}}$ plane to a similar sub-percent accuracy [124,125].

Large size of current and future surveys, with millions and up to a billion of observed galaxies, *requires* the use of photometric redshifts. These photometric redshifts will be calibrated by obtaining spectra of a subset of galaxies, and “training” the photometric spectra using the spectroscopic subset. Of order 10^5 spectra seem to be required for future surveys [122,93,126,124], although this number strongly depends on the expected scatter in the photometric redshifts around the true value and other details. Moreover, the spectroscopic galaxies need to be a representative sample of the

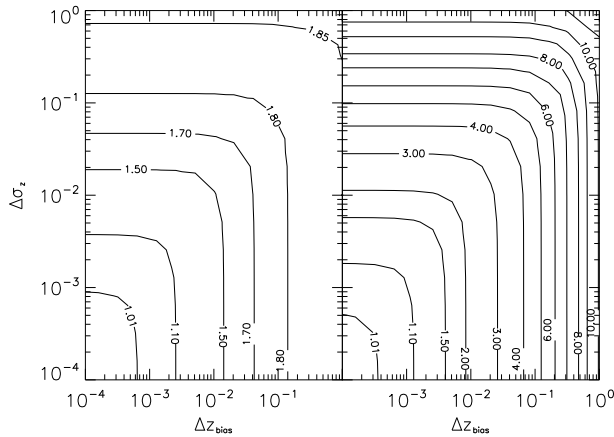


Fig. 8 Requirements on the accuracy of photometric redshifts to perform weak lensing tomography, adopted from Ref. [122]. Contours show error degradations in constant w (left panel) and those in w_a (when where both w_0 and w_a are varied; right panel), as a function of prior knowledge of the mean (x-axis) and scatter (y-axis) in the relation between the true (spectroscopic) and photometric redshift. The degradations are defined as actual errors in cosmological parameters relative to the errors with perfectly known photometric redshifts. For example, the right panel shows that no more than 50% degradation (factor 1.5 on the contours) in the error in w_a requires knowledge of the photometric redshift mean and scatter to better than ~ 0.003 in each redshift bin.

whole population — for example, very high redshift galaxies in the survey need to be represented in the spectroscopic subsample — and this adds another layer of challenge to the program of photometric redshift calibration.

Errors on the observed shapes of galaxies are manifold, and include imperfect knowledge of the point-spread function, atmospheric blurring, thermal and mechanical effects of the telescope, etc. More generally, errors in measurements of galaxy shear can be described as either additive or multiplicative errors [127]. The measured shear of source galaxies at redshift z_s and in direction \mathbf{n} , $\hat{\gamma}(z_s, \mathbf{n})$, can be written as

$$\hat{\gamma}(z_s, \mathbf{n}) = \gamma(z_s, \mathbf{n}) \times [1 + f_i(z_s, \mathbf{n})] + \gamma_{\text{add}}(z_s, \mathbf{n}) \quad (23)$$

where $\gamma(z_s, \mathbf{n})$ is the true shear, $f_i(z_s, \mathbf{n})$ is the multiplicative and $\gamma_{\text{add}}(z_s, \mathbf{n})$ the additive error ([127]; see also [128]). Multiplicative errors can be caused by, for example, finite size of the point-spread function with which the galaxy image is convolved while additive errors can be created, for example, by atmospheric blurring. The requirements are stringent; for example, future surveys need to calibrate the mean multiplicative errors to about 0.1% (i.e. $\delta f_i \approx 0.001$) accuracy in each of ~ 10 redshift bins in order that dark energy constraints not be significantly degraded [127]. However, what really helps weak lensing is the possibility of “self-calibrating” the systematic errors — determining a reasonable set of the systematic error nuisance parameters from the survey concurrently with the cosmological parameters without appreciable degradation in accuracy on the latter [127, 129, 130]. With self-calibration, the survey itself is used to partially calibrate the systematic effects.

7.2 Theoretical modeling systematics

Predicting the weak lensing shear power spectrum requires knowledge of the dark matter power spectrum (see Eq. 12); intrinsic uncertainty in predicting the power spectrum *in the nonlinear regime* (on scales $\ell \gtrsim 200$, or below about 1 degree) constitutes the principal theoretical weak lensing systematic. Ref. [131] found that power spectrum on scales of ~ 1 Mpc (corresponding roughly to a few arcminutes on the sky), where weak lensing measurements are most accurate, needs to be calibrated to a few percent. While not trivial, this accuracy seems within reach due to recent impressive progress in obtaining precision results from large numerical simulations (e.g. [132]).

One additional difficulty, currently only partially explored, is how the addition of gas to pure dark matter simulations affects the results; it appears that baryonic physics can be phenomenologically modeled with sufficient accuracy [133, 134, 135]. Another challenge to theoretical predictions is that a large suite of numerical simulations appears necessary to cover the multi-dimensional cosmological parameter space; fortunately, clever statistical techniques can be employed to cover the parameter space so that a very reasonable total number of simulations (~ 100) is sufficient [136, 137].

Weak lensing provides a large amount of information, given by shapes and redshifts of millions (or, in the future, billions) of galaxies. Therefore, there is redundancy in weak lensing measurements that can be used to minimize the effect of systematic errors with negligible degradation in the statistical errors on cosmological parameters. For example, by taking only the *cross*-power spectra for cosmology ($P_{ij}^{\kappa}(\ell)$ with $i \neq j$ in Eq. (12)), one can minimize biases due to correlations between intrinsic galaxy ellipticities [138] (see also [139]). Similarly, one can perform “nulling tomography” of weak lensing to selectively throw out the small-scale information in the convergence power spectrum that is most sensitive to the unwanted biases [140].

8 Conclusions

Weak lensing probes dark matter and energy in the universe in multiple ways. With galaxy-galaxy lensing, it probes the structure of individual dark matter halos. With detecting galaxy clusters from the shear of the foreground galaxies, it enables the cosmological number-count test that is sensitive to distances and growth of density perturbations, and thus to temporal evolution of dark energy. And with measuring the correlation of shear signal across the sky, weak lensing again probes distances and growth, but now with a completely different set of statistical and systematic errors.

In this review article, we briefly covered the aforementioned cosmological uses of weak lensing; we did not mention some related topics that are covered elsewhere in this Special Issue (for example, lensing of the CMB [141]). We also emphasized the intrinsic power of weak lensing, and the potential of weak lensing to self-calibrate an impressive range of systematic errors and still produce excellent cosmological constraints. This situation can perhaps be contrasted with strong gravitational lensing, where only a modest number of multiply imaged systems (~ 100) is currently available, and where it is important to have very precise *a-priori* constraints on the systematic effects in order to extract the cosmologically interesting information.

Current efforts in weak lensing research emphasize performing observations with ever wider and deeper surveys, improving the accuracy and reliability of weak lensing measurements, improving the understanding of nonlinear clustering of dark matter

and baryons with N-body simulations, and devising clever methods to self-calibrate the systematic errors and measure new properties of dark energy and modified gravity. If these efforts continue at the current rate of progress, weak lensing is likely to firmly establish itself as one of the most reliable and powerful probes of dark energy and matter in the universe.

Acknowledgements I would like to thank Jörg Dietrich and Alexie Leauthaud for useful comments on the earlier version of Sec. 3, and Alexie Leauthaud for kindly providing Fig. 3. My work is supported by the DOE OJI grant under contract DE-FG02-95ER40899, NSF under contract AST-0807564, and NASA under contract NNX09AC89G.

References

1. J.A. Tyson, R.A. Wenk, F. Valdes, *Astrophys. J. Lett.* **349**, L1 (1990)
2. T.G. Brainerd, R.D. Blandford, I. Smail, *Astrophys. J.* **466**, 623 (1996)
3. J. Miralda-Escude, *Astrophys. J.* **380**, 1 (1991)
4. N. Kaiser, *Astrophys. J.* **388**, 272 (1992)
5. B. Jain, U. Seljak, *Astrophys. J.* **484**, 560 (1997)
6. F. Bernardeau, L. Van Waerbeke, Y. Mellier, *Astron. Astrophys.* **322**, 1 (1997)
7. N. Kaiser, *Astrophys. J.* **498**, 26 (1998)
8. M. Kamionkowski, A. Babul, C.M. Cress, A. Refregier, *Mon. Not. Roy. Astron. Soc.* **301**, 1064 (1998)
9. L. Hui, *Astrophys. J.* **519**, L9 (1999)
10. D.J. Bacon, A.R. Refregier, R.S. Ellis, *Mon. Not. Roy. Astron. Soc.* **318**, 625 (2000)
11. N. Kaiser, G. Wilson, G.A. Luppino, *astro-ph/0003338* (2000)
12. L. van Waerbeke, et al., *Astron. Astrophys.* **358**, 30 (2000)
13. D.M. Wittman, J.A. Tyson, D. Kirkman, I. Dell'Antonio, G. Bernstein, *Nature* **405**, 143 (2000)
14. J. Frieman, M. Turner, D. Huterer, *Ann. Rev. Astron. Astrophys.* **46**, 385 (2008)
15. Y. Mellier, *astro-ph/9901116* (1999)
16. M. Bartelmann, P. Schneider, *Phys. Rept.* **340**, 291 (2001)
17. A. Refregier, *Ann. Rev. Astron. Astrophys.* **41**, 645 (2003)
18. D. Munshi, P. Valageas, L. Van Waerbeke, A. Heavens, *Phys. Rept.* **462**, 67 (2008)
19. H. Hoekstra, B. Jain, *Annual Review of Nuclear and Particle Science* **58**, 99 (2008)
20. W. Hu, M.J. White, *Astrophys. J.* **554**, 67 (2001)
21. C. Shapiro, *Astrophys. J.* **696**, 775 (2009)
22. C. Heymans, et al., *Mon. Not. Roy. Astron. Soc.* **368**, 1323 (2006)
23. R. Massey, et al., *Mon. Not. Roy. Astron. Soc.* **376**, 13 (2007)
24. W. Hu, *Astrophys. J.* **522**, L21 (1999)
25. P. Abell, et al., 0912.0201 (2009)
26. A. Cooray, W. Hu, *Astrophys. J.* **548**, 7 (2001)
27. P. Schneider, M. Lombardi, *Astron. Astrophys.* **397**, 809 (2003)
28. P. Schneider, M. Kilbinger, M. Lombardi, *Astron. Astrophys.* **431**, 9 (2005)
29. M. Takada, B. Jain, *Mon. Not. Roy. Astron. Soc.* **344**, 857 (2003)
30. S. Dodelson, P. Zhang, *Phys. Rev. D* **72**(8), 083001 (2005)
31. F. Bernardeau, Y. Mellier, L. van Waerbeke, *Astron. Astrophys.* **389**, l28 (2002)
32. U.L. Pen, et al., *Astrophys. J.* **592**, 664 (2003)
33. E. Semboloni, et al., 1005.4941 (2010)
34. M. Takada, B. Jain, *Mon. Not. Roy. Astron. Soc.* **348**, 897 (2004)
35. M. Takada, S. Bridle, *New J. Phys.* **9**, 446 (2007)
36. P. Fischer, et al., *Astron. J.* **120**, 1198 (2000)
37. T.A. McKay, et al., *astro-ph/0108013* (2001)
38. H. Hoekstra, H.K.C. Yee, M.D. Gladders, *Astrophys. J.* **606**, 67 (2004)
39. R. Mandelbaum, U. Seljak, G. Kauffmann, C.M. Hirata, J. Brinkmann, *Mon. Not. Roy. Astron. Soc.* **368**, 715 (2006)
40. G. Wilson, N. Kaiser, G.A. Luppino, L.L. Cowie, *Astrophys. J.* **555**, 572 (2001)
41. E.S. Sheldon, et al., *Astron. J.* **127**, 2544 (2004)

-
42. D.E. Johnston, et al., *Astrophys. J.* **656**, 27 (2007)
 43. J. Guzik, U. Seljak, *Mon. Not. Roy. Astron. Soc.* **335**, 311 (2002)
 44. A. Leauthaud, et al., *Astrophys. J. Suppl.* **172**, 219 (2007)
 45. A. Leauthaud, et al., in preparation
 46. M. Kleinheinrich, P. Schneider, H. Rix, T. Erben, C. Wolf, M. Schirmer, K. Meisenheimer, A. Borch, S. Dye, Z. Kovacs, L. Wisotzki, *Astron. Astrophys.* **455**, 441 (2006)
 47. R. Mandelbaum, et al., *Mon. Not. Roy. Astron. Soc.* **372**, 758 (2006)
 48. D.E. Johnston, et al., arXiv:0709.1159 (2007)
 49. A. Leauthaud, et al., *Astrophys. J.* **709**, 97 (2010)
 50. E.S. Sheldon, et al., *Astrophys. J.* **703**, 2232 (2009)
 51. W. Hu, B. Jain, *Phys. Rev.* **D70**, 043009 (2004)
 52. F. Schmidt, *Phys. Rev.* **D78**, 043002 (2008)
 53. D. Wittman, J.A. Tyson, V.E. Margoniner, J.G. Cohen, I.P. Dell'Antonio, *Astrophys. J.* **557**, L89 (2001)
 54. D. Wittman, V.E. Margoniner, J.A. Tyson, J.G. Cohen, I.P. Dell'Antonio, *Astrophys. J.* **597**, 218 (2003)
 55. D. Wittman, et al., *Astrophys. J.* **643**, 128 (2006)
 56. M. Schirmer, T. Erben, M. Hettterscheidt, P. Schneider, *Astron. Astrophys.* **462**, 875 (2007)
 57. J.P. Dietrich, T. Erben, G. Lamer, P. Schneider, A. Schwobe, J. Hartlap, M. Maturi, *Astron. Astrophys.* **470**, 821 (2007)
 58. S. Miyazaki, T. Hamana, R.S. Ellis, N. Kashikawa, R.J. Massey, J. Taylor, A. Refregier, *Astrophys. J.* **669**, 714 (2007)
 59. D. Clowe, et al., *Astrophys. J.* **648**, L109 (2006)
 60. L. Mariani, G.M. Bernstein, *Phys. Rev.* **D73**, 123525 (2006)
 61. W.J. Fang, Z. Haiman, *Phys. Rev.* **D75**, 043010 (2007)
 62. W. Hu, C.R. Keeton, *Phys. Rev.* **D66**, 063506 (2002)
 63. M.J. White, L. van Waerbeke, J. Mackey, *Astrophys. J.* **575**, 640 (2002)
 64. N. Padmanabhan, U. Seljak, U.L. Pen, *New Astron.* **8**, 581 (2003)
 65. T. Hamana, M. Takada, N. Yoshida, *Mon. Not. Roy. Astron. Soc.* **350**, 893 (2004)
 66. J.F. Hennawi, D.N. Spergel, *Astrophys. J.* **624**, 59 (2005)
 67. L. Mariani, R.E. Smith, G.M. Bernstein, *Astrophys. J.* **698**, L33 (2009)
 68. J.P. Dietrich, J. Hartlap, *Mon. Not. Roy. Astron. Soc.* **in press** (2010)
 69. J.M. Kratochvil, Z. Haiman, M. May, *Phys. Rev.* **D81**, 043519 (2010)
 70. H. Dahle, *Astrophys. J.* **653**, 954 (2006)
 71. E. Rozo, et al., *Astrophys. J.* **708**, 645 (2010)
 72. M. Jarvis, G.M. Bernstein, P. Fischer, D. Smith, B. Jain, J.A. Tyson, D. Wittman, *Astron. J.* **125**, 1014 (2003)
 73. M.L. Brown, et al., *Mon. Not. Roy. Astron. Soc.* **341**, 100 (2003)
 74. H. Hoekstra, H.K.C. Yee, M.D. Gladders, L.F. Barrientos, P.B. Hall, L. Infante, *Astrophys. J.* **572**, 55 (2002)
 75. L. Van Waerbeke, Y. Mellier, H. Hoekstra, *Astron. Astrophys.* **429**, 75 (2005)
 76. H. Hoekstra, Y. Mellier, L. van Waerbeke, E. Semboloni, L. Fu, M.J. Hudson, L.C. Parker, I. Tereno, K. Benabed, *Astrophys. J.* **647**, 116 (2006)
 77. M. Hettterscheidt, P. Simon, M. Schirmer, H. Hildebrandt, T. Schrabback, T. Erben, P. Schneider, *Astron. Astrophys.* **468**, 859 (2007)
 78. J. Benjamin, et al., *Mon. Not. Roy. Astron. Soc.* **381**, 702 (2007)
 79. A. Refregier, J. Rhodes, E.J. Groth, *Astrophys. J.* **572**, L131 (2002)
 80. J. Rhodes, et al., *Astrophys. J.* **605**, 29 (2004)
 81. R. Massey, et al., *Nature* **445**, 286 (2007)
 82. M. Kilbinger, et al., *Astron. Astrophys.* **497**, 677 (2009)
 83. R. Massey, et al., *Astrophys. J. Suppl.* **172**, 239 (2007)
 84. L. Fu, et al., *Astron. Astrophys.* **479**, 9 (2008)
 85. D.N. Spergel, et al., *Astrophys. J. Suppl.* **170**, 377 (2007)
 86. M. Jarvis, B. Jain, G. Bernstein, D. Dolney, *Astrophys. J.* **644**, 71 (2006)
 87. C. Schimd, et al., *Astron. Astrophys.* **463**, 405 (2007)
 88. W. Hu, M. Tegmark, *Astrophys. J.* **514**, L65 (1999)
 89. D. Huterer, *Phys. Rev.* **D65**, 063001 (2002)
 90. P. Simon, L.J. King, P. Schneider, *Astron. Astrophys.* **417**, 873 (2004)
 91. D. Munshi, P. Valageas, astro-ph/0510266 (2005)
 92. A.F. Heavens, T.D. Kitching, A.N. Taylor, *Mon. Not. Roy. Astron. Soc.* **373**, 105 (2006)

-
93. A. Amara, A. Refregier, *Mon. Not. Roy. Astron. Soc.* **381**, 1018 (2007)
 94. H. Zhan, L. Knox, *astro-ph/0611159* (2006)
 95. C. Shapiro, S. Dodelson, *Phys. Rev.* **D76**, 083515 (2007)
 96. G.M. Bernstein, *Astrophys. J.* **695**, 652 (2009)
 97. G. Aldering, et al., *astro-ph/0405232* (2004)
 98. G.M. Bernstein, B. Jain, *Astrophys. J.* **600**, 17 (2004)
 99. B. Jain, A. Taylor, *Phys. Rev. Lett.* **91**, 141302 (2003)
 100. J. Zhang, L. Hui, A. Stebbins, *Astrophys. J.* **635**, 806 (2005)
 101. G. Bernstein, *Astrophys. J.* **637**, 598 (2006)
 102. A.N. Taylor, T.D. Kitching, D.J. Bacon, A.F. Heavens, *Mon. Not. Roy. Astron. Soc.* **374**, 1377 (2007)
 103. D. Huterer, E.V. Linder, *Phys. Rev.* **D75**, 023519 (2007)
 104. J.P. Uzan, F. Bernardeau, *Phys. Rev.* **D64**, 083004 (2001)
 105. B. Jain, P. Zhang, *Phys. Rev.* **D78**, 063503 (2008)
 106. J.P. Uzan, *arXiv:0908.2243* (2009)
 107. E.V. Linder, *Phys. Rev.* **D72**(4), 043529 (2005)
 108. E.V. Linder, R.N. Cahn, *Astroparticle Physics* **28**, 481 (2007)
 109. G.R. Dvali, G. Gabadadze, M. Porrati, *Phys. Lett.* **B485**, 208 (2000)
 110. M. Ishak, A. Upadhye, D.N. Spergel, *Phys. Rev.* **D74**, 043513 (2006)
 111. S.F. Daniel, R.R. Caldwell, A. Cooray, A. Melchiorri, *Phys. Rev. D* **77**(10), 103513 (2008)
 112. L. Amendola, M. Kunz, D. Sapone, *Journal of Cosmology and Astro-Particle Physics* **4**, 13 (2008)
 113. O. Doré, et al., *arXiv:0712.1599* (2007)
 114. M.J. White, C.S. Kochanek, *Astrophys. J.* **560**, 539 (2001)
 115. R. Reyes, et al., *Nature* **464**, 256 (2010)
 116. F. Schmidt, *Phys. Rev.* **D78**, 043002 (2008)
 117. H. Zhan, L. Knox, J.A. Tyson, *Astrophys. J.* **690**, 923 (2009)
 118. P. Zhang, R. Bean, M. Liguori, S. Dodelson, *arXiv:0809.2836* (2008)
 119. G.B. Zhao, L. Pogosian, A. Silvestri, J. Zylberberg, *Phys. Rev.* **D79**, 083513 (2009)
 120. A. Cooray, D. Holz, D. Huterer, *Astrophys. J.* **637**, L77 (2006)
 121. S. Dodelson, A. Vallinotto, *Phys. Rev.* **D74**, 063515 (2006)
 122. Z.M. Ma, W. Hu, D. Huterer, *Astrophys. J.* **636**, 21 (2005)
 123. H. Oyaizu, M. Lima, C.E. Cunha, H. Lin, J. Frieman, *Astrophys. J.* **689**, 709 (2008)
 124. G. Bernstein, D. Huterer, *Mon. Not. Roy. Astron. Soc.* **401**, 1399 (2010)
 125. A.P. Hearin, A.R. Zentner, Z. Ma, D. Huterer, *arXiv:1002.3383* (2010)
 126. Z. Ma, G. Bernstein, *Astrophys. J.* **682**, 39 (2008)
 127. D. Huterer, M. Takada, G. Bernstein, B. Jain, *Mon. Not. Roy. Astron. Soc.* **366**, 101 (2006)
 128. T.D. Kitching, A.N. Taylor, A.F. Heavens, *Mon. Not. Roy. Astron. Soc.* **389**, 173 (2008)
 129. P. Zhang, *arXiv:0811.0613* (2008)
 130. P. Zhang, U.L. Pen, G. Bernstein, *arXiv:0910.4181* (2009)
 131. D. Huterer, M. Takada, *Astropart. Phys.* **23**, 369 (2005)
 132. K. Heitmann, P.M. Ricker, M.S. Warren, S. Habib, *Astrophys. J. Suppl.* **160**, 28 (2005)
 133. D.H. Rudd, A.R. Zentner, A.V. Kravtsov, *Astrophys. J.* **672**, 19 (2008)
 134. A.R. Zentner, D.H. Rudd, W. Hu, *Phys. Rev.* **D77**, 043507 (2008)
 135. A.P. Hearin, A.R. Zentner, *Journal of Cosmology and Astro-Particle Physics* **4**, 32 (2009)
 136. K. Heitmann, D. Higdon, C. Nakhleh, S. Habib, *Astrophys. J.* **646**, L1 (2006)
 137. K. Heitmann, et al., *Astrophys. J.* **705**, 156 (2009)
 138. M. Takada, M.J. White, *Astrophys. J.* **601**, L1 (2004)
 139. B. Joachimi, P. Schneider, *Astron. Astrophys.* **488**, 829 (2008)
 140. D. Huterer, M.J. White, *Phys. Rev.* **D72**, 043002 (2005)
 141. D. Hanson, A. Challinor, A. Lewis, *arXiv:0911.0612* (2009)